Depth profiling using XPS
by Stephen Michael Hunt

A thesis submitted in partial fulfillment Of the requirements for the degree of Master of Science in Chemical Engineering
Montana State University

Abstract:
Angle resolved X-ray photoelectron spectroscopy (ARXPS) is now one of the most widely used surface analysis techniques in research because it supplies an abundance of surface, chemical and electronic information. A major limitation of conventional XPS is that sample concentrations are calculated based on the assumption that the elemental concentrations are homogeneous in the outer 100 &aring:, an assumption that is frequently inaccurate. By exploiting the angular dependence of the XPS sampling depth, it is easy to get a qualitative assessment of surface uniformity. The objective of this work has been to explore the limits to which ARXPS data can be used for quantitative estimation of the depth profile.

Calculating depth/concentration profiles for ARXPS data is a mathematically unstable problem. This means that relatively small errors in the data can propagate into rather large errors in the calculated profiles. It can therefore be inferred that the method used to obtain the approximation greatly influences the error in calculated profiles.

This study has investigated two algorithms that can be used to calculate depth profiles from ARXPS data: Tyler Regularization and Singular Value Decomposition.

The influences of random error and surface roughness have been investigated.

Simulations have been used to quantify how different types of error propagate through the calculations. Optimum parameters for ARXPS experiments and the calculations have been identified. The results have been validated on a series of samples consisting of self-assembled monolayers.

Random error studies suggest that the calculated depth profiles are only semi-quantitative. The accuracy and resolution of the calculated profiles is strongly influenced by the selection of smoothing parameters. Optimum smoothing parameters for different error levels in the measured data have been recommended. Improved accuracy was observed when the number of angles used in the calculations was increased from three to five but no improvement was observed by further increasing the number of angles to 10. Simulations also indicate that surface roughness has a minimal effect except at glancing angles. Based on the calculations, it is recommended that measurements be taken at 10°, 20°, 40°, 50°, and 70°.

DEPTH PROFILING USING XPS

By

Stephen Michael Hunt

A thesis submitted in partial fulfillment
Of the requirements for the degree

of

Master of Science

in

Chemical Engineering

MONTANA STATE UNIVERSITY – BOZEMAN
Bozeman, Montana

April 2000

APPROVAL

of a thesis submitted by

Stephen Michael Hunt

This thesis has been read by each member of the thesis committee and has been found to be satisfactory regarding content, English usage, format, citations, bibliographic style, and consistency, and is ready for submission to the College of Graduate Studies.

Dr. Bonnie J. Tyler _____ April 14, 2000
(Signature) Date

Approved for the Department of Chemical Engineering

Dr. John T. Sears _____ April 14, 2000
(Signature) Date

Approved for the College of Graduate Studies

Dr. Bruce McLeod _____ 4-14-00
(Signature) Date

STATEMENT OF PERMISSION TO USE

In presenting this thesis in partial fulfillment of the requirements for the master's degree at Montana State University-Bozeman, I agree that the library shall make it available to borrowers under the rules of the library.

If I have indicated my intention to copyright this thesis by including a copyright notice page, copying is allowable only for scholarly purposes, consistent with the "fair use" as prescribed in the U.S. Copyright Law. Requests for permission for extended quotation from or reproduction of this thesis in whole or in parts may be granted only by the copyright holder.

Signature 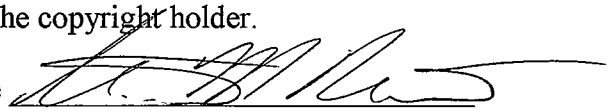

Date April 14, 2000

This work is dedicated to my wife Dana. If not for her untiring love, patience, and support, this work would not be possible.

TABLE OF CONTENTS

LIST OF TABLES

LIST OF TABLES - CONTINUED

LIST OF TABLES - CONTINUED

LIST OF TABLES - CONTINUED

LIST OF FIGURES

LIST OF FIGURES - CONTINUED

LIST OF FIGURES - CONTINUED

LIST OF FIGURES - CONTINUED

LIST OF FIGURES - CONTINUED

ABSTRACT

Angle resolved X-ray photoelectron spectroscopy (ARXPS) is now one of the most widely used surface analysis techniques in research because it supplies an abundance of surface, chemical and electronic information. A major limitation of conventional XPS is that sample concentrations are calculated based on the assumption that the elemental concentrations are homogeneous in the outer 100 Å, an assumption that is frequently inaccurate. By exploiting the angular dependence of the XPS sampling depth, it is easy to get a qualitative assessment of surface uniformity. The objective of this work has been to explore the limits to which ARXPS data can be used for quantitative estimation of the depth profile.

Calculating depth/concentration profiles for ARXPS data is a mathematically unstable problem. This means that relatively small errors in the data can propagate into rather large errors in the calculated profiles. It can therefore be inferred that the method used to obtain the approximation greatly influences the error in calculated profiles.

This study has investigated two algorithms that can be used to calculate depth profiles from ARXPS data: Tyler Regularization and Singular Value Decomposition. The influences of random error and surface roughness have been investigated. Simulations have been used to quantify how different types of error propagate through the calculations. Optimum parameters for ARXPS experiments and the calculations have been identified. The results have been validated on a series of samples consisting of self-assembled monolayers.

Random error studies suggest that the calculated depth profiles are only semi-quantitative. The accuracy and resolution of the calculated profiles is strongly influenced by the selection of smoothing parameters. Optimum smoothing parameters for different error levels in the measured data have been recommended. Improved accuracy was observed when the number of angles used in the calculations was increased from three to five but no improvement was observed by further increasing the number of angles to 10. Simulations also indicate that surface roughness has a minimal effect except at glancing angles. Based on the calculations, it is recommended that measurements be taken at 10°, 20°, 40°, 50°, and 70°.

CHAPTER 1

INTRODUCTION

Conventional X-ray photoelectron spectroscopy (XPS) provides identification of all elements (except H and He) present in outermost 100Å in concentrations greater than 0.1atomic percent. A major limitation in this technique is that sample concentrations are calculated as a weighed average of concentrations, which implies the elemental concentrations are homogeneous in this region [1]. By exploiting the angular dependence of sampling depth as illustrated in Figure 1, it is possible to get a qualitative assessment of surface uniformity. This is the basis of angle resolved X-ray photoelectron spectroscopy (ARXPS). ARXPS in now one of the most widely used surface analysis techniques in research because it supplies an abundance of surface, chemical and electronic information [2, 3].

Obtaining a quantitative assessment of the depth/concentration profile poses formidable mathematical difficulties. The depth/concentration profile in the upper approximately 100Å has important implications in the study of adhesion, catalysis, composite materials, corrosion, microelectronics, and self-assembling monolayers. In many instances, other surface sensitive techniques cannot be used either because of the destructive nature of the technique or the inability of the technique to provide adequate

depth resolution. Therefore, particular attention has been paid to ARXPS as a tool for obtaining quantitative estimates of concentration profiles in the near surface region.

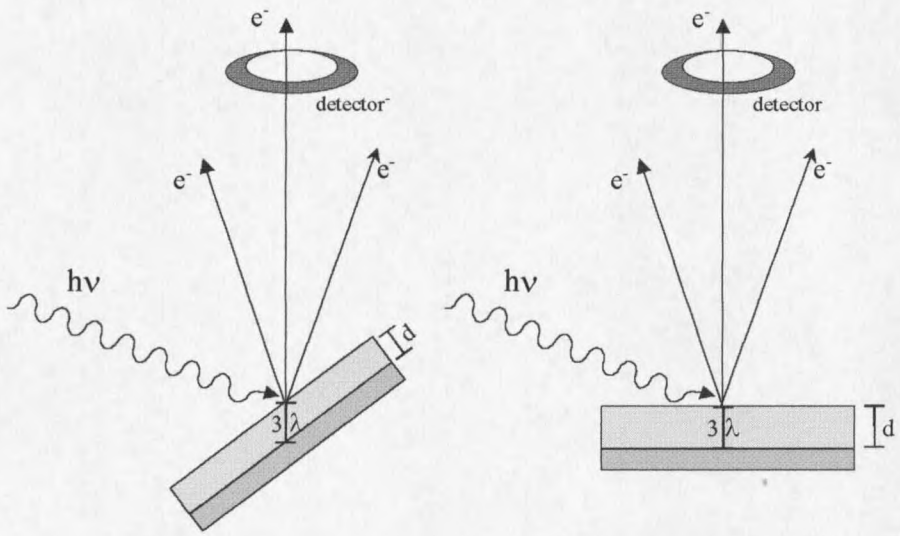

Figure 1. Cartoon Illustrating the Angle Dependence on Sampling Depth

Problems in this Area

Calculating depth/concentration profiles for ARXPS data is a mathematically unstable problem. This can be translated to mean that relatively small errors in the data can propagate into rather large errors in the calculated profiles. Therefore, specialized numerical methods have been developed to approximate the profiles. In general, the method must augment the ARXPS data generated with some prior knowledge of the nature of the solution [4]. This prior knowledge is then used in some manner to restore lost data. However, as one attempts to be more rigorous in the approximation of the

profile, the more the mathematical instability interferes with the solution [5]. It can therefore be inferred that the method used to obtain the approximation greatly influences the error in calculated profiles.

The expression for the intensity of the photoelectron flux as a function of take off angle, from any orbital of an element, has been reduced to a Laplace transform with certain assumptions to produce depth profiles [6-8]. Bussing and Holloway have shown that a unique solution to the inverse Laplace transform is unattainable and suggested that any solution is a selection from a class of equivalent solutions [6-8]. The inverse Laplace transform also takes the form of a class of ill-posed problems commonly referred to as Fredholm Integral of the first kind [5]. Solutions to Fredholm Integrals of the first kind typically employ methods derived from inverse theory. As might be expected, the solution to this expression has been approached with a multitude of methods.

Motivation for Research

The typical x-ray source used in XPS irradiates approximately an 800μm x 800μm spot on the sample surface [3]. As might be expected surface roughness can greatly influence the signal generated by varying the angle between the x-ray source and sample. This affects the effective sampling depth (Figure 1) and introduces systematic error into the data collected. Hence, ARXPS is generally not regarded as useful tool for generating concentration profiles on rough samples.

Secondly, by changing the take-off angle, angle between the source and surface normal, the effective sampling depth is altered (Figure 1). Displayed in Figure 1, this

technique generates a significantly more intense signal from the atoms closest to the surface. The sampling depth is proportional to the mean free path of an escaping electron and the cosine of the angle between the analyzer input axis and sample surface normal. A large angle restricts analysis to the uppermost layers, while small angles ($\approx 0^{\circ}$-10°) can give information from 12-15 atomic layers down.

It is important to understand that by changing the take-off angle you are not viewing different slices of the sample. Therefore, experiments conducted at various take-off angles are only suggestive of a concentration profile. The concern here is how this affects the resolution of deeper features in the approximated concentration profile.

Obviously, surface roughness and signal intensity is a result of the sample and technique used in analysis; not the method used to approximate the profile. However, the method used to calculate the profiles and their associated parameters greatly influences how these problems filter through to the approximated concentration profile.

Research Objectives

- To understand uniform error propagation when calculating concentration depth profiles from angle resolved x-ray photoelectron spectra using the following algorithms: Tyler Regularization and Singular Value Decomposition. Particularly as it related to accuracy of the overlayer thickness, overlayer composition, gradient of the interface, and substrate composition.
- To determine the effect of surface roughness on measured signal intensities and calculated profiles.
- To determine optimal experimental and algorithmic parameters for the Tyler Regularization Algorithm and Singular Value Decomposition Algorithm.

- Verify findings by collecting XPS data on self-assembling monolayers (SAMs).

CHAPTER 2

BACKGROUND

Conventional X-ray Photoelectron Spectroscopy

Conventional X-ray Photoelectron Spectroscopy is an information-rich technique (Table 1). However, it is important to understand that the level of sophistication used in interpretation of the data determines the detail of the chemistry, organization and morphology that can then be analyzed. This versatility makes it the most widely used surface characterization technique in research [2].

Theory and Principle

A fundamental understanding of the photoelectric effect and the photoemmision process is indispensable to the understanding of XPS. When a surface is irradiated by a photon one of three things can happen: 1) the photon can pass through, 2) the photon can interact with an atomic orbital electron yielding partial energy loss, or 3) the photon can interact with an atomic orbital electron with total energy loss. It is this third process, displayed in Figure 2, that is primary to XPS. When a given photon impinges upon an atom, electrons will be ejected (photoemision) given that the frequency of excitation is

greater than some threshold level distinctive to each element. This ejected electron will then possess some kinetic energy, KE, which can then be measured.

Table 1. Information Derived from an XPS experiment from Ratner and Castner [1]

In the outermost 10nm of a surface, XPS can provide

- Identification of all elements (except H and He) present at concentrations >0.1 atomic percent
- Semi-quantitative determination of the approximate elemental surface composition (error $< \pm 10\%$)
- Information about the molecular environment (oxidation state, bonding atoms, etc.)
- Information about aromatic or unsaturated structures from shakeup ($\pi^* \rightarrow \pi$) transitions
- Identification of organic groups using derivatization reactions
- Non-destructive elemental depth profiles 10nm into the sample and surface heterogeneity assessment using (1) angular dependant XPS studies and (2) photoelectrons with differing escape depths
- Destructive elemental depth profiles several hundred nanometers into the sample using ion etching (for inorganics)
- Laterial variations in surface composition (spatial resolution of 8-150μm, depending upon the instrument)
- 'Fingerprinting' of materials using valence band spectra and identification of bonding orbitals
- Studies on hydrated (frozen) surfaces

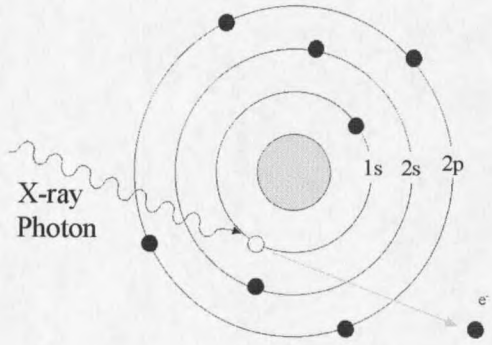

Figure 2. Cartoon of an atom undergoing photoemmision

The binding energy can then be calculated according to the following equation:

$$E_B = h\upsilon - KE \tag{1}$$

where E_B is the binding energy of the electron and hν is the energy of the X-ray source. With hν being a known quantity and the ability to accurately measure KE it is possible to calculate the binding energy, which is directly related to the type of atom and the molecular environment from which the electron came.

Quantitation of Conventional XPS Data

To quantify data from an XPS spectrum the intensity of the inelastically scattered electrons (total number of electrons emitted that have lost no energy) are calculated by integrating the area underneath the peak representing each specific element. The common equation used to describe the photoelectron intensity as a function of elemental concentration is given by:

$$F_{i,j}^{*}(\theta) = \frac{A \cdot \sigma_{i,j} \cdot \Psi}{\sin\phi} \cdot \int_0^{\infty} \eta_j(x) \cdot e^{\frac{-x}{\lambda_{i,j} \cdot \cos\theta}} dx \tag{2}$$

where $F_{i,j}^{*}$ is the absolute signal intensity of peak i of the j^{th} element in the sample; A is a constant that includes X-ray flux, area of the sample being irradiated, and the detector efficiency; $\sigma_{i,j}$ is the photoinization cross-section, ψ is the transmission function of the detector; ϕ is the angle between the X-ray and the surface; θ is the angle between the surface normal and the photoelectron electron trajectory; $n_j(x)$ is the concentration of element j at a depth x; and λ is the electron attenuation length (i.e,. the distance an electron can travel before being elastically scattered). Commonly, the normalized signal intensity is used and can be calculated by correcting for differences in the photoinization cross-section, transmission function, sampling depth and changes in X-ray incidence.

$$F_{i,j}(\theta) = F_{i,j}^{*}(\theta) \cdot \left(\frac{\sigma_{i,j} \cdot \Psi \cdot \lambda_{i,j}}{\sin \phi} \right)^{-1} = \frac{A}{\lambda_{i,j}} \cdot \int_{0}^{\infty} \eta_j(x) \cdot e^{\frac{-x}{\lambda_{i,j} \cdot \cos\theta}} dx \qquad (3)$$

It is common in XPS to define a new variable in order to reduce the number of unknowns in Equation 3. This is accomplished by defining the relative composition, $n_{i,j}(x)$ as

$$n_{i,j}(x) = A \cdot \eta_j \qquad (4)$$

The relative composition reduces Equation 3 to an equation with one unknown as follows:

$$F(\theta) = \int_{0}^{\infty} n_{i,j}(x) \cdot e^{\frac{-x}{\lambda_{i,j} \cdot \cos\theta}} dx \qquad (5)$$

For conventional XPS, Equation 5 is further simplified by assuming all elemental concentrations are homogeneous throughout the XPS sampling depth. This allows Equation 3 to be integrated to obtain:

$$F_{i,j}(\theta) = n_{i,j} \cdot \cos(\theta) \tag{6}$$

Calculation of the atomic percentages is then:

$$\eta_j = 100\left(\frac{\eta_{i,j}}{\sum_{k=1}^{m}\eta_{i,k}}\right) \tag{7}$$

It is important to note that if the concentration is not homogeneous in the sampling depth Equation 4 is not valid and Equation 3 must be used in conjunction with a smoothing technique as discussed in the next section. Homogeneity is typically determined qualitatively by performing experiments at different take-off angles, θ, which effectively changes the sampling depth as displayed in Figure 1.

Angle Resolved X-ray Photoelectron Spectroscopy

Obtaining a quantitative concentration profile when the sampling depth is not homogeneous is not mathematically straightforward. Equation 3 is a Laplace transform of the depth profile of the concentration profile, $n_j(x)$. Bussing and Holloway have shown that inverse transforming finite sets of data does not produce unique solutions, rather any solution is a selection from a class of equivalent solutions ranging from smooth to highly oscillatory [6-8].

The Laplace transform in Equation 5 is in the form of one general class of ill-posed problems commonly referred to as a Fredholm integral of the first kind[9]. These equations take the following form:

$$F(\theta) = \int_0^\infty n(x) \cdot K(x,\theta) \cdot dx \tag{8}$$

where F(θ) is the known "right-hand side" and n(x) the unknown function to be solved. The function of two variables is commonly referred to as the Kernel and is generally derived from theory. For calculating concentration profiles $K(x,\theta) = \exp(-x/\lambda\cos(\theta))$. Equation 8 is analogous to the matrix equation:

$$K \cdot n = F \tag{9}$$

It should be apparent that this is an "ill posed" problem, in that we are attempting to reconstruct a whole function from a finite number of discrete points. Applying the Kernel to a function is generally regarded as a smoothing operation, so the solution, which requires inverting the operator, will be extremely sensitive to small changes or errors in the input. That is to say, oscillations in the solution, n(x), are observed when simply minimizing the sum of squared errors as follows:

$$\varphi(n) = \left\| \int_0^\infty n(x) \cdot K(x,\theta) dx - F(\theta) \right\|^2 \tag{10}$$

Most algorithms have utilized iterative approaches that forward transforms a hypothetical $n_{i,j}(x)$ and optimizes the calculated intensities, F(θ), subject to some constraints. This optimization typically stabilizes the solution when calculated according to Equation 10. A common constraint is to restrict the atomic percentages to be physically realistic (i.e. 0%-100%). However, additional constraints tend to considerably limit the form of the resulting concentration profiles. Methods that employ inverse

theory have been used successfully, two of which will be discussed below; the Singular Value Decomposition algorithm and the Tyler Regularization algorithm.

The Tyler Algorithm

Tikhonov proposed in the early 1960's that Equation 10 might be replaced with a similar equation as follows [5, 10]:

$$\varphi(n) = \left\| \int_0^\infty n(x) \cdot K(x,\theta)dx - F(\theta) \right\|^2 + \alpha \cdot g(n) \qquad (11)$$

where α is a positive numerical operator or smoothing parameter. Tikhonov set $g(n)=\|n(x)\|^2$ where Tyler sets $g(n)=\|n(x)K(x,\theta)\|^2$ which is equivalent to $\|n(x)\|^2$ under certain conditions. Using the relationship that increasing α pulls the solution away from minimizing the first term in Equation 11 in favor of minimizing $\alpha\|n(x)\|^2$.

This method attempts to minimize two positive functionals. The first measures the agreement of the model to the data. When done alone, the agreement between the model and the data becomes very good, however, the solution becomes unstable, oscillatory, or just unrealistic. This defines the first term alone as a highly degenerate minimization problem. The second term in Equation 11 is typically referred to as a stabilizing functional or regularizing operator. The regularizing operator measures the "smoothness" in the desired solution. Therefore minimizing the regularizing operator alone gives a stable or likely solution that may have no correlation to the measured data.

Equation 11 is a Fredholm integral equation of the second kind and has stable, unique minimums for values of α greater than zero. It can be readily observed that

Equation 10 is simply a limiting case of Equation 11 and as α approaches zero the solution to Equation 11 approaches that of Equation 10. Choosing an appropriate value for α that is large enough to stabilize the problem without "smoothing out" any of the real features is then of principal concern for obtaining a realistic solution.

A method of applying non-negativity constraints to Fredholm Integrals of the first kind was developed by Butler, Reeds, and Dawson in the early 1980's [11]. Britten, Travis, and Brown demonstrated that by constraining the solution, n(x), to be physically realistic (i.e., non-negative) the solution could be further stabilized and greatly improved the agreement between postulated and calculated distributions [12]. Tyler later presented a modified version of the Butler, Reeds and Dawson algorithm for solution to Fredholm Integral Equations of the first kind as they apply to the approximation of concentration profiles [5]. It is this approach, presented by Tyler, which will be used in this work.

It has been shown that for a particular smoothing parameter, α, the solution, n(x), can be solved for by minimizing Equation 11. Equation 11 has been shown to have a unique minimum, which is readily found by setting the gradient equal to zero as follows [11]:

$$\nabla\varphi = K(x,\theta)\left[\int_0^\infty n(x)\cdot K(x,\theta)dx - F(\theta)\right] + \alpha K = 0 \qquad (12)$$

If the solution, n(x), can be expressed as a linear of functions such that:

$$n(x) = \max\left[0, \sum_i^n c_i \cdot e^{\frac{-x}{SF\cos\theta}}\right], \quad \text{where } SF = 1.5\cdot\max(\lambda) \qquad (13)$$

$$n(x) = \max\left[0, \sum_i^n c_i x^i\right], \text{ or} \qquad (14)$$

$$n(x) = \max\left[0, \sum_{i}^{n} c_i \cdot \cos(\omega \cdot x)\right] \qquad \text{where} \quad \omega = \frac{\pi}{180 \cdot 2^i}, \text{ or} \tag{15}$$

$$n(x) = \max\left[0, \sum_{i}^{n} c_i \sum_{m=0}^{M} \frac{(2i-2m)!}{2^i m!(i-m)!(i-2m)!} x^{i-2m}\right] \tag{16}$$

where M = i/2, or (n-1)/2 whichever is an integer

where,

$$K(x,\theta) = e^{\frac{-x}{\lambda \cos\theta}} \tag{17}$$

If we then define a new variable M such that:

$$M_{i,j} = \int_D K(x,\theta_i) \cdot K(x,\theta_j) dx \tag{18}$$

D= all intervals on which n(x)>0

Equation 11 can then be rewritten as follows:

$$(M + \alpha I)c = F \tag{19}$$

The Tyler algorithm applies a non-negativity constraint iteratively. M is initially calculated over the interval of 0 to ∞ to generate an estimate of c. The estimate of the solution, n(x), is then calculated according to Equation 13. M is then recalculated only over the intervals for which the approximating function is non-negative. The process is repeated until:

$$\frac{\|(M + \alpha I)c - F\|}{\|F\|} \leq 10^{-6} \tag{20}$$

Singular Value Decomposition

The second method used in this work to approximate concentration profiles from ARXPS data uses Singular Value Decomposition (SVD) to solve the inverse problem. This can be regarded as a general linear least squares problem as in Equation 10 or a limiting case of the Tyler Algorithm. For all practical purposes, we will consider it a limiting case of the Tyler algorithm with α equal to zero, and solve by the method outlined in the previous section.

As mentioned above, Equation 19 with α equal to zero is an unstable problem. The matrix M is typically very close to singular in which case a zero pivot element may be encountered resulting in no solution. Alternatively, a very small pivot may be encountered, which leads to fit parameters with very large magnitudes that are balanced to cancel out almost precisely when the function is evaluated. SVD overcomes this problem by allowing the user to remove possible singularities and inverting M in Equation 15. This enables calculation of the vector c as follows:

$$c = V \cdot \left[diag\left(1/w_j\right) \right] \cdot \left(U^T \cdot F \right) \tag{21}$$

where,

$$M = \begin{pmatrix} & & \\ & \mathrm{U} & \\ & & \end{pmatrix} \cdot \begin{pmatrix} w_1 & & & \\ & w_2 & & \\ & & \vdots & \\ & & & w_j \end{pmatrix} \cdot \begin{pmatrix} & & \\ & \mathrm{V^T} & \\ & & \end{pmatrix} \tag{22}$$

In Equation 21 and 22 U is an i x j matrix whose columns are orthonormal, W is an j x j matrix with positive or zero elements (the singular values), and V is a j x j orthogonal matrix. The decomposition in Equation 22 can always be done regardless of how close to

singular the M matrix is. If F lies within the range of M the singular set of equations has an solution (in fact is has more than one solution since any vector in the null space can be added to c in any linear combination) when calculated by Equation 21. If F does not lie within the range of M the singular set of equations has no solution. However, Equation 21 will construct the closest solution in a least squares sense.

The SVD algorithm overcomes the singularity or near singularity problem as follows: if any singular value w_j is zero, its reciprocal in Equation 21 is set to zero as opposed to infinity. Similarly, if any singular value w_j is near zero, it is also is set to zero. This corresponds to adding to the fitted parameters c a zero multiple, as opposed to some random large multiple, of any linear combination of basis functions that are degenerate in the fit [4]. Editing additional singular values (not close to zero) can also identify additional linear combinations of variables that do not greatly affect the minimization of Equation 11. However, this is beyond the scope of this work.

This algorithm, implemented similar to the Tyler algorithm above, has three notable differences: α is set equal to zero, the matrix inversion is done using singular value decomposition, and the adjustable parameter is the number of singular values used. By adjusting the number of singular values, w_j's, used it effectively smoothes or dampens the approximated solution, n(x) (e.g. the more singular values used the more unstable the solution).

Atomic Force Microscopy

Binnig, Quate and Gerber first introduced atomic force microscopy in 1986 as a new instrument for examining the surfaces of thin insulated crystals [13]. It operates under the same principles as the record player or reading Braille just on a smaller scale.

The Atomic Force Microscope (AFM) probes the surface of a sample with a sharp tip, approximately 240μm long, 2.5μm thick, and often less than 20μm in diameter [3]. The tip is located at the free end of a cantilever as shown in Figure 3. Forces between the surface and tip cause the cantilever to deflect; this deflection is then measured using a laser photodiode detector. The detector electronics then produce a map of the surface topography. The measured signal is then used to control movements of the piezoelectric crystal on which the cantilever is mounted, via a feed back loop (Figure 3).

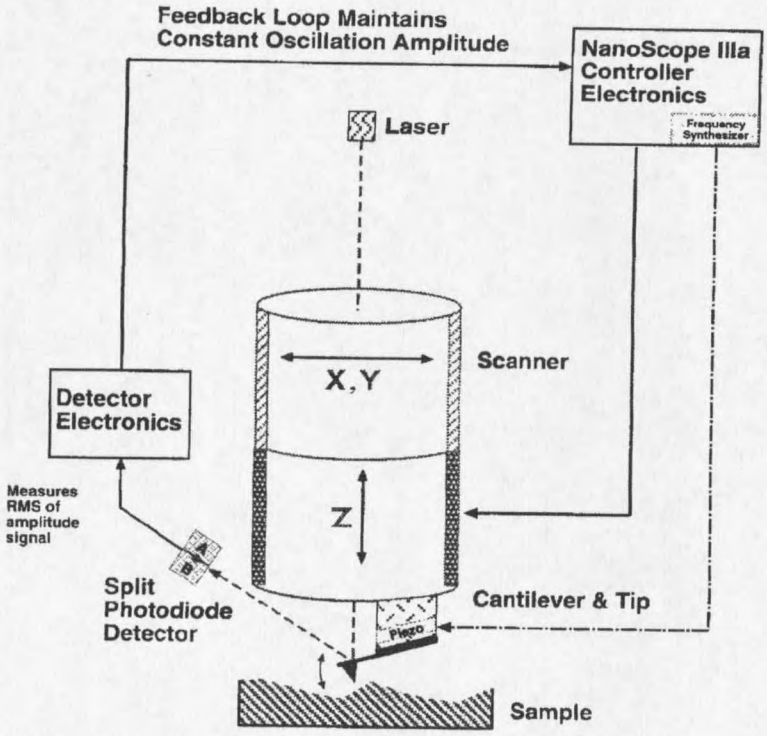

Figure 3. Schematic of Tapping™ Mode AFM [14]

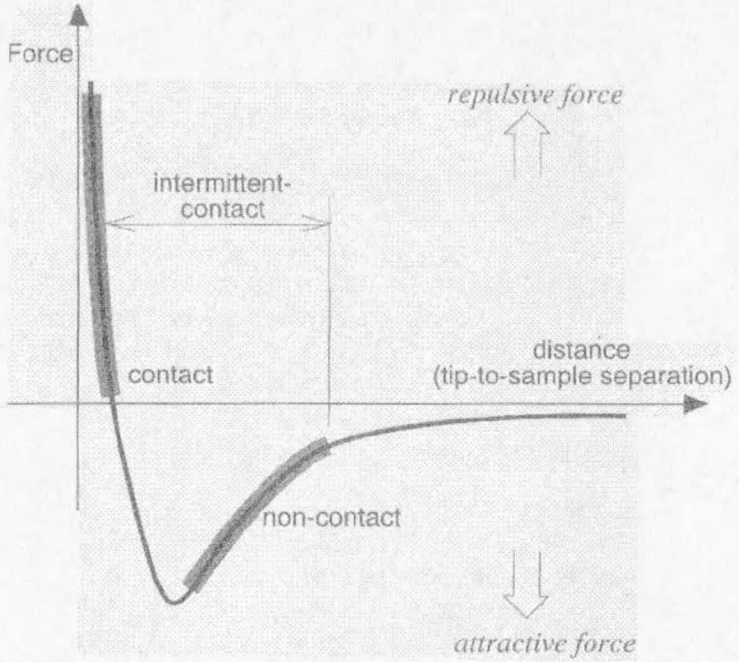

Figure 4. Relationship Between van der Waals Force and Tip to Surface Distance [15]

There are three primary modes in which the AFM is capable of operating: Contact Mode, Non-contact Mode, and Tapping™ Mode. The advantages and disadvantages of each are summarized in Table 2. The AFM has two principal modes of interaction between the tip and sample: attractive and repulsive. Figure 4 demonstrates this dependence of van der Waals force on tip to sample distance and the corresponding tip interaction associated with each type of experiment.

Contact Mode AFM operates under the principle that as the cantilever pushes the tip to the sample, the cantilever flexes as opposed to forcing the tip atoms closer to the sample atoms. This can be seen in the slope of the curve in Figure 4 in the contact regime. Rather than decreasing interatomic distances, the surface is likely to deform instead [15]. Only in contact mode is the AFM able to achieve atomic resolution [14]. Other forces on cantilever which can contribute in contact mode are lateral forces, capillary forces and the force exerted by the cantilever itself [15].

Table 2. Advantages and Disadvantages of Contact Mode AFM, Tapping mode AFM, and Non-contact Mode AFM [14].

Contact Mode AFM

Advantages:

- High scan speeds (throughput)
- Contact mode AFM is the only AFM technique that can obtain "atomic resolution" images.
- Rough samples with extreme changes in vertical topography can sometimes be scanned more easily in contact mode.

Disadvantages:

- Lateral (shear) forces can distort features in the image.
- The forces normal to the tip-sample interaction can be high in air due to capillary forces from the absorbed fluid layer in the sample surface.
- The combination of lateral forces and high normal forces can result in reduced spatial resolution and may damage soft samples (i.e., biological samples, polymers, and silicon) due to scraping between the tip and sample.

Non-contact Mode AFM

Advantage:

- No force exerted on the sample surface.

Disadvantages:

- Lower lateral resolution, limited by the tip-sample separation
- Slower scan speed than Tapping Mode and Contact Mode to avoid contacting the absorbed fluid layer, which results in the tip getting stuck.
- Non-contact usually only works on extremely hydrophobic samples, where the absorbed fluid layer is at a minimum. If the fluid layer is too thick, the tip becomes trapped in the absorbed fluid layer causing unstable feedback and scraping of the sample.

Tapping Mode AFM

Advantages:

- Higher lateral resolution on most samples (1nm to 5nm).
- Lower forces and less damage to soft samples imaged in air.
- Lateral forces are virtually eliminated, so there is no scraping.

Disadvantages:

- Slightly slower scan speed than contact mode AFM.

Due to these disadvantages, applications for non-contact mode AFM *imaging have been limited.*

Non-contact mode AFM is, generally speaking, more suited for analyzing soft or elastic samples. In non-contact mode, the cantilever is vibrated near its resonant frequency (about 100-400kHz) with an amplitude on the order of a 10-100Å [15]. However, because the total force between the tip and sample is very low in this regime as seen in Figure 4, difficulties are often encountered when collecting an image.

The third mode typically available in atomic force microscopy is Tapping™ mode or intermittent-contact mode. This mode operates under the same principle as non-contact AFM except the tip is brought close enough to the sample that it just barely touches the surface. Again the system detects deviations in amplitude of the cantilever when vibrating near its resonant frequency. Tapping™ mode AFM nearly eliminates the lateral forces seen in contact mode and has been found to be more effective for imaging larger areas that have larger variance in surface features than non-contact mode [15].

Self-Assembling Monolayers

Self-assembled monolayers (SAMs) have attracted much attention as a model system for the study of thin-film organic materials. The interest in the properties of these thin-film organic materials is due to the wide range of applications now being discovered: supramolecular assembly, wetting, tribology, biological interfaces, electrochemistry, corrosion inhibition, etc.

Particular attention, however, has been paid to SAMs consisting of n-alkane thiols adsorbed on gold. This system has been proven to be thermally stable, well ordered, and can easily be made using ω-substituted thiols to modify surface properties. The

overlayers are formed in a simple, near equilibrium procedure. They also exhibit strong adsorbate-substrate bonding and, for n>5, the chain-terminating group has no knowledge of the underlying gold substrate. Gold is used as the substrate because it is reasonably inert and allows for manipulation in air with lessened concern for contamination. Few functional groups besides thiols (or disulfides which dissociate upon adsorption) bind strongly to gold.

Samples are generally prepared using a mica wafers primed with an adhesion layer of ~40Å of titanium. The gold (>2000Å) is then deposited by e-beam evaporation onto the wafers. Samples are then immersed in ethanol solutions of the adsorbate (~10^{-1} M) contained in glass jars (no precautions are generally used to exclude air). The reaction is believed to proceed as followoms:

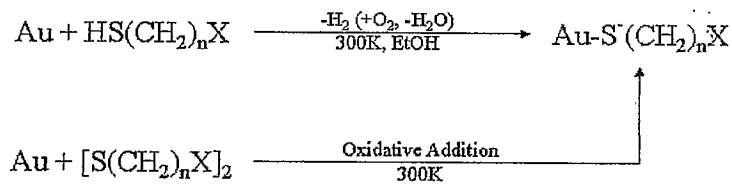

(23)

Previous studies have established that this procedure produces polycrystalline gold films exhibiting a strong (111) texture and grains >1000Å in size [16]. These dense monolayers assemble rather quickly, however well ordered systems can take days to form. It is the understanding of the author that the less ordered the system the more susceptible the samples are to oxidation in air.

CHAPTER 3

EXPERIMENTAL

Computer Simulated Data

Because this is an ill-posed problem, conventional methods for determining error propagation cannot be utilized. It is the purpose of this work to place an upper bound on how the error in the initial data propagates through the calculations. Although the algorithms are being evaluated on computer simulated data with known amounts of error, this is still an ill-posed problem and does not make the solution any more stable.

Flat Surface

The computer generated data was simulated by integrating Equation 5 for a number of profiles, n(x). The data consisted of four components in two layers as displayed in Figure 5. Each layer consisted of a 1:5 mixture of two hypothetical elements with inelastic mean free paths, λ, of 30Å. Uniformly distributed error of 1%, 2%, and 5% was also introduced to the data. Depth profiles were then calculated using each algorithm from data sets consisting of three take-off angles (10°, 40°, & 80°), five take-off angles (10°, 20°, 40°, 60°, & 80°) and ten take-off angles (10°, 20°, 30°, 40°, 50°, 60°, 65°, 70°, 75°, & 80°).

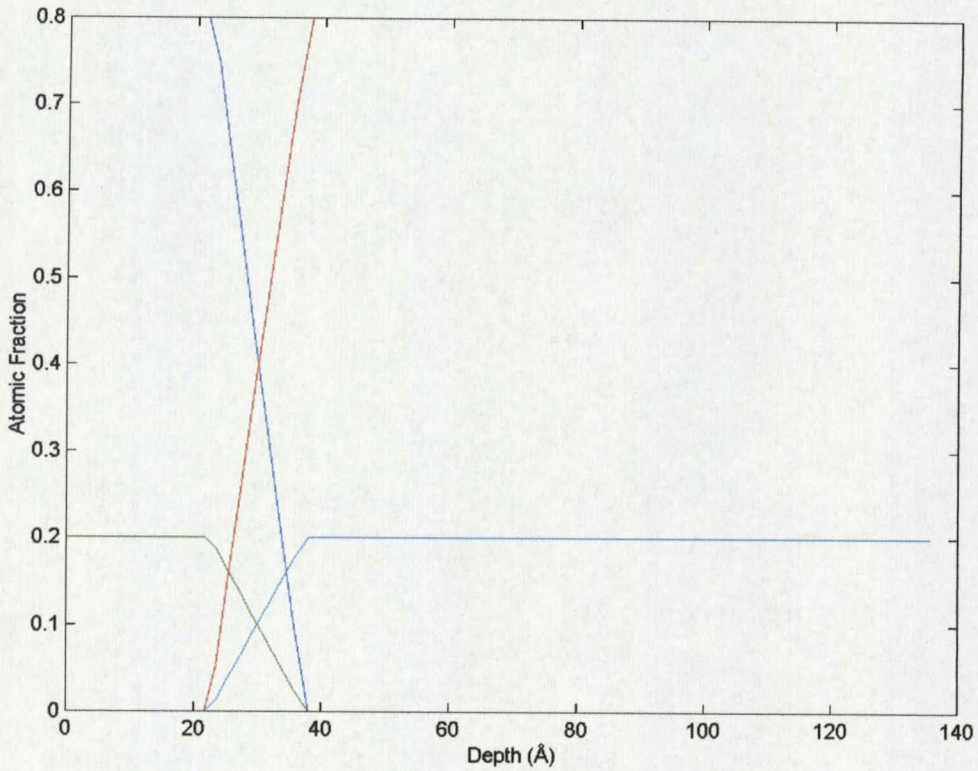

Figure 5. Example of Profile Used to Generate Computer Simulated Data

In order to determine the effect of depth of an interface on accuracy, resolution and stability data was simulated at four different depths: $\lambda/4$, $\lambda/2$, λ, and 2λ. At each depth the gradient of the interface was changed to help determine how large changes in the shape in the interface must be to resolve them from other gradients. The different slopes and gradients used are shown in Figures 6-10:

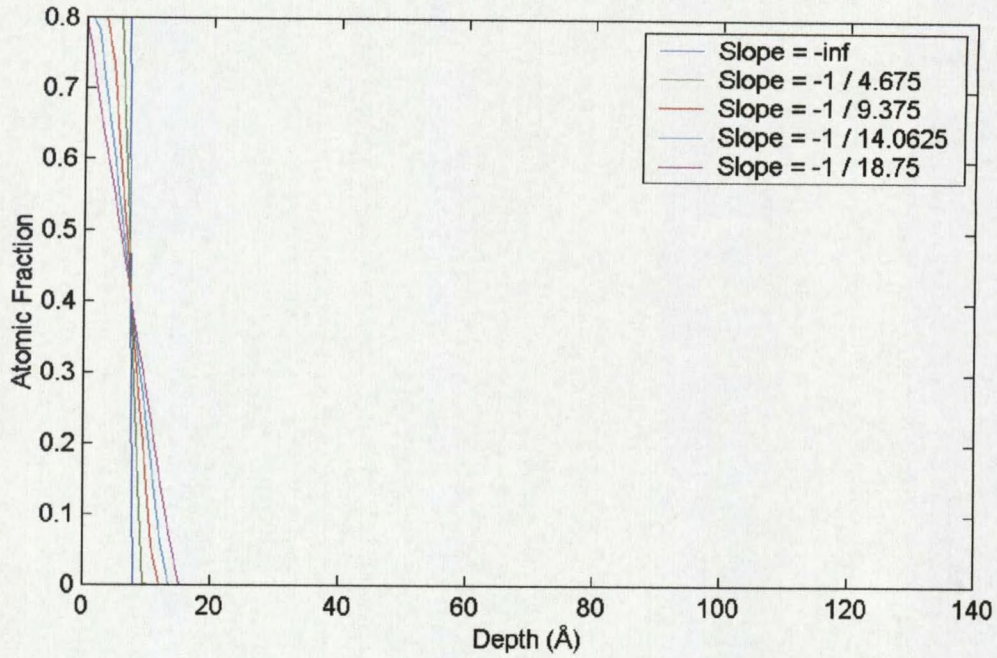

Figure 6. Simulated Data with a λ/4 Overlayer

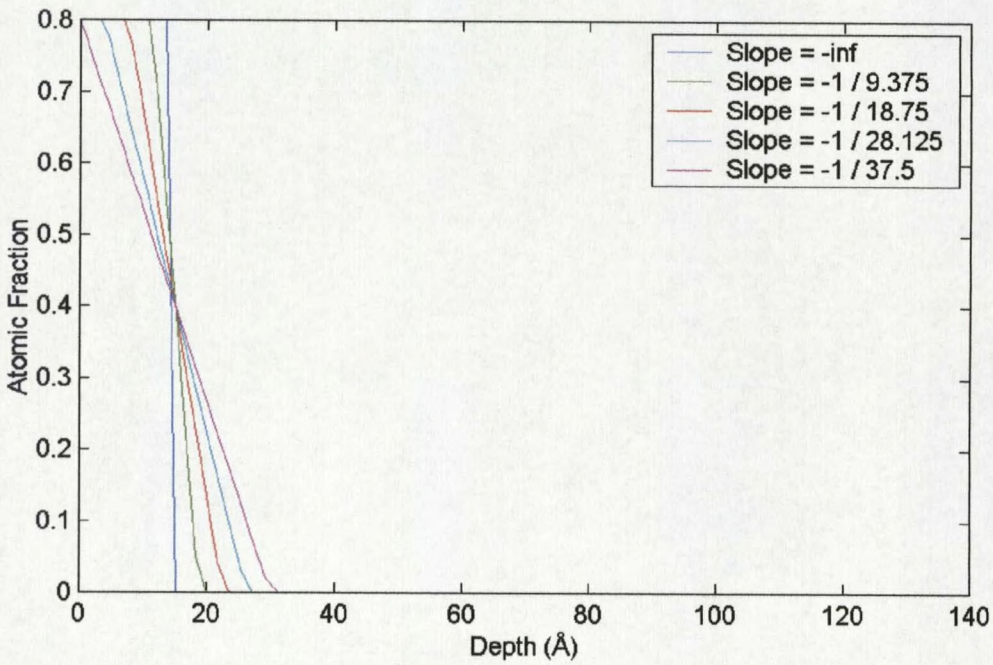

Figure 7. Simulated Data with a λ/2 Overlayer

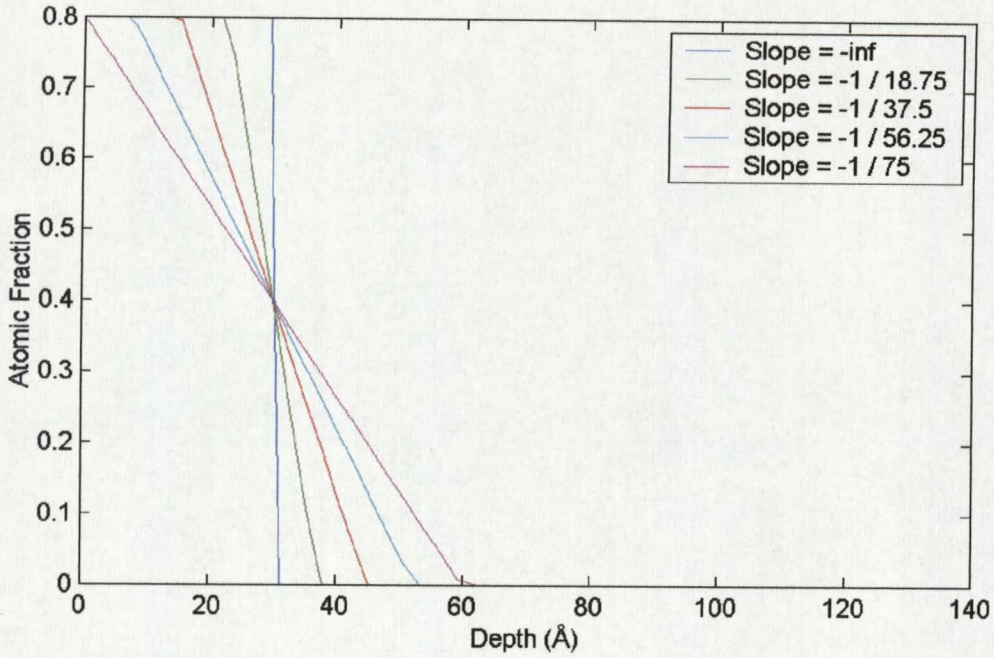

Figure 8. Simulated Data with a 1λ Overlayer

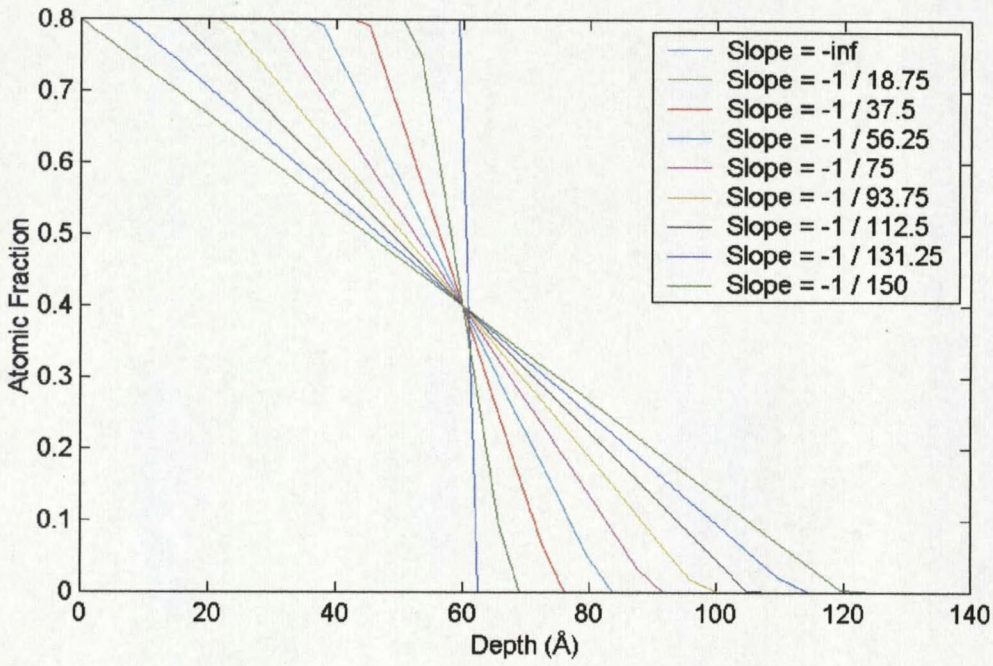

Figure 9. Simulated Data with a 2λ Overlayer

Simulated Rough Surface

Data was also simulated for three-dimensional wavelike surfaces of varying amplitude. This was accomplished by generating a mesh surface according to the following equation:

$$H = A\cos(x)\cos(y)\Big|_{x=0\ldots 2\pi, y=0\ldots 2\pi} \tag{24}$$

where H is the height of the surface and A is an adjustable parameter that varies the amplitude to period ratio. The x and y gradients were calculated and the appropriate adjustments were made to the take-off angle to impose a 1λ overlayer on the surface. This was done as follows:

$$\phi = a\tan\left(\frac{\partial H}{\partial x}\right), \qquad \beta = a\tan\left(\frac{\partial H}{\partial y}\right) \tag{25 \& 26}$$

$$\theta_{actual} = \frac{1}{\sqrt{1+\tan^2(\theta+\phi)}\sqrt{1+\tan^2(\beta)}} \tag{27}$$

where θ_{actual} is the actual angle between the surface normal. The corresponding intensities, $F(\theta_{actual})$, were then calculated for each point on the 150x150 wavelike grid. The average intensity for each take-off angle was then calculated for use in both the Tyler Regularization and SVD methods. Again, three data sets using three, five and ten measurements as described above were used to test the algorithms.

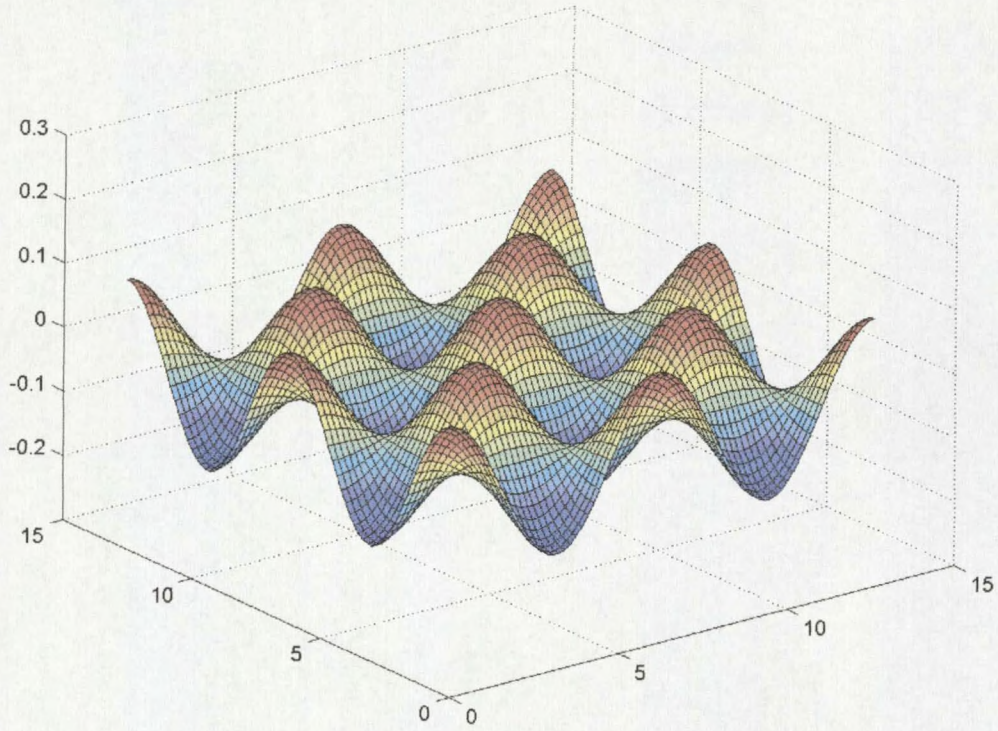

Figure 10. Example of the Wavelike Surface

Fourteen values for A in Equation 24 were chosen (0.02, 0.04…0.28). The A values were chosen to correspond to the same magnitude of the samples on which data was collected experimentally. Roughness is defined as the ratio of the actual surface area to the area of the projected surface. This was calculated for the simulated data as follows:

$$\frac{SA}{PSA} = (2\pi)^{-2} \int\int \sqrt{\left(-A\sin(x)\cos(y)\right)^2 + \left(-A\cos(x)\sin(y)\right)^2 + \left(-1\right)^2}\, dydx \qquad (28)$$

Profile Approximation

Profiles for all the simulated data were approximated using both the Tyler Regularization and SVD algorithms. For the Tyler Regularization algorithm the profiles were approximated using 20 different smoothing parameters, α, corresponding to Equation 29.

$$\alpha = 1.8^{1-n} \qquad n=1,2\ldots20 \qquad (29)$$

The SVD algorithm approximated the profiles using between one and one less than the number of take-off angles used. Data were simulated using both the exponential (Equation 13) and the power (Equation 14) approximation functions. The data for each were stored on compact disk for further analysis. Cosine (Equation 15) and Legendre polynomial (Equation 16) approximating functions were also attempted. These functions produced highly unstable solutions, and therefore, no further analysis was attempted.

Experimentally Collected Data

Duplicate samples of three chain length alkanethiols (C8, C12, and C16) were prepared at the University of Washington and sent Montana State University for analysis. The samples were prepared by vapor deposition of > 200Å of gold onto a clean mica wafer that had been primed with an adhesion layer of ~ 40Å of titanium. The samples were then immersed in 20mM ethanol solutions of the C8, C12, or C16 thiol adsorbate contained in glass jars and shipped to Montana State University. Upon receiving of the samples (~ 3 days after submersion) they were rinsed with an ethanol solution, placed in separate containers, labeled, and stored under a constant N_2 purge.

XPS Spectra were collected using a Physical Electronics Instrument Model 5600 spectrometer at ten take-off angles (10°, 20°, 30°, 40°, 50°, 60°, 65°, 70°, 75°, & 80°). Spectra were obtained from two spots on each sample. The SAMs were mounted on a sample holder using both double-sided adhesive tape and copper arms attached to the sample holder. They were then placed into a vacuum chamber at a pressure of $\sim 10^{-8}$ mmHg. An 800μm-diameter area was irradiated using a monochromatized 0.2mm aluminum kα X-ray source at 300 watts. The pass energies used for all elements during data acquisition were 117.40eV. The XPS spectra were integrated using MultiPak ® Version 2.2 distributed by Physical Electronics to produce the signal intensities. The intensities were normalized under the assumptions of equal inelastic mean free paths and constant density to remove any instrument variation. The resulting scaled intensities were then used in both the Tyler Regularization and SVD algorithms.

The profiles for the data were approximated using subsets of three angles, five angles and the full data set. The optimal adjustable parameter (α and number of singular values) for each overlayer thickness and interface gradient were determined by these simulated data experiments.

The topography of each sample was determined using a Digital Instruments Dimension 3100 Series Scanning Probe Microscope in tapping mode AFM. The AFM analyses were performed using a $1\mu m^2$, $100\mu m^2$, and $2500\mu m^2$ scan area at a scan rate of ~ 1Hz. The surface area of each scan was determined using 3100 Series software. The ratio of the surface area to the area of the projected surface was then calculated.

CHAPTER 4

OPTIMUM SMOOTHING AND ASSOCIATED STABILITY

As previously mentioned the algorithms will be evaluated using three criteria: stability, accuracy, and resolution. The first step in the analysis of the simulated data is to determine the optimum smoothing parameter (α) or number of singular values used for each combination of depth and gradient. This enables comparison of the best data sets (according to the selection criteria) for each depth and gradient. The selection criterion is the mean squared error of the profile.

$$\varepsilon = \left\| True\ \text{Pr}ofile - Calculated\ \text{Pr}ofile \right\| \tag{30}$$

Three primary gradients (infinite, $^{-1}/_{18.75}$, and $^{-1}/_{37.5}$) will be discussed extensively. This will enable a closer comparison of the different interface depths. Although the discussion will focus primarily on these three gradients, any trends discussed apply to all gradients unless otherwise noted.

Tyler Regularization

Exponential Approximating Function

Table 3 summarizes the optimum smoothing parameters for the Regularization Algorithm using the Kernel function as the approximating function. (Tables and Figures are located at the end of the chapter.) General trends can be observed from this data. The most predominant trend in the data set is the value of the optimum smoothing parameter increases with increasing data set error. Also, the optimum value of the smoothing parameter tends to decrease with increasing depth of the interface, and increase slightly as the gradient deviates from infinity. The relationship between the number of measurements and optimum smoothing value displays negligible difference between those with five measurements and those with ten measurements. However, when only three measurements are used, the optimum smoothing parameter is smaller than the optimum for cases using more measurements. The above generalizations are not, however, without exception.

The associated stability data for the optimized α values are located in Table 4. The stability of the algorithm at the optimal smoothing parameter decreases as the percent error in the data decreases. This counterintuitive result arises because a smaller smoothing parameter is used when smaller error is introduced into the data. Thus, by increasing the smoothing parameter convergence would be improved. This was confirmed by re-computing the percentage converged for all error levels (0%, 1%, 2%,

and 5%) using the largest optimum smoothing parameter from each depth and gradient as illustrated in Figures 11 and 12.

Another interesting trait of the Tyler Regularization Method is that a plot of error (as defined by Equation 30) against the smoothing parameter (α) shows that there is a very broad minimum. This suggests that the depth profile is not sensitive to small variations in the smoothing parameter. This trend is shown for the case using five measurements in Figures 13-17 and is seen in the cases with three and ten measurements.

For typical real XPS data, the actual profile is not known and the best smoothing must be found using other criteria. The method typically used by Tyler is displayed in Equation 31.

$$\varepsilon = \left\| NF_{Calculated} - NF_{Input} \right\| \tag{31}$$

Where NF_{Input} is the normalized ARXPS signal intensities, and $NF_{Calculated}$ is the normalized intensity data calculated using Equation 5 with the approximated profile as n(x). Each element is normalized with respect to its highest signal intensity over all take-off angles.

The optimum smoothing parameters and corresponding stability data can be found in Tables 5 and 6. Similarly, the same type of broad minimum previously mentioned can be seen for all depths and gradients. An interesting feature observed when comparing the smoothing parameters from both methods is that the smoothing parameter selected using Equation 31 is smaller than that found when using Equation 30 at shallow interfaces and larger than that found using Equation 30 when observing deeper features. It appears that the two methods will predict the same smoothing parameter when features are between

15Å and 30Å. Another interesting feature is that the gradient does not seem to affect the selection of the smoothing parameter. These trends are displayed in Figures 16 and 17, where the line is the smoothing parameter selected using Equation 30 and the attached circular marker is that selected by predictive optimum (Equation 31).

It is expected that the predictive criterion (Equation 31) is more sensitive to the upper 30Å of the approximated profile. This will be explored in the next chapter

Power Approximating Function

The data for the optimum smoothing value and corresponding stability for use of the Regularization algorithm with the power approximating function (Equation 14) data

$$n(x) = \max\left[0, \sum_{i}^{n} c_i x^i\right] \tag{14}$$

is shown in Table 7 and 8. The most obvious aspect of this data set is its instability. This is most likely a result of the magnitude ratio between the largest and smallest terms ($c \cdot x^n$: $c \cdot x$) in Equation 14. This will cause the matrix $\mathbf{M}$ in Equation 18 to approach singularity and thus the solution to be highly oscillatory. Even in the cases where the ratio is at its smallest (3 measurements) the stability data is not favorable. Therefore, it can be concluded that Equation 14 is not a viable alternative to Equation 13 in the Tyler Regularization Algorithm.

Singular Value Decomposition

Exponential Approximating Function

Tables 9 and 10 summarize the optimum number of singular values and the associated stability data for the SVD Algorithm as selected by Equation 30 using the kernal as the approximating function. It should be reiterated that the stability data in Table 10 reflects the stability of the method with the smoothing and not the actual method. From the data it is inferred that the optimum number of singular values used in calculation goes through a maximum as the depth of the interface increases. The gradient has no considerable effect on the number of singular values when the interface is near the surface. As the features become deeper in the sample (>30Å) the optimum number of singular values decreases as the interface becomes more abrupt. The relationship between the number of measurements and number of singular values used does not provide any noticeable trends other than the number used with ten measurements is almost equal to that when five measurements are used. This possibly indicates that ten measurements may provide little additional information to five measurements.

A noteworthy concern, however, is that when this algorithm uses too few singular values (one and possibly two) the model does not represent the actual data. Similar to Tyler Regularization, a plot of the mean squared error (Equation 30) against the optimum number of singular values again displays a broad minimum which may indicate the true optimum may be any value in the range of integers shown in Figure 18. This is alarming

when observing (Table 9) the cases that used 5 and 10 measurements with the optimum numbers typically between 2-3 singular values when error is present.

When the predictive criteria (Equation 31) of selecting the optimum number of singular values is used there appears to be little discrepancy from the mean squared error in the approximated profile (Equation 30) for interfaces near the surface (Figure19). However at deeper interfaces, there is a notable discrepancy at low error levels and gradual interfaces (Figure 30). This discrepancy reveals that the predicted optimum tends to be less than the actual optimum. Again, the optimum number of singular values may be any one of a series of integers due the relatively flat minimum when plotted against the predicted error.

Power Approximating Function

Tables 13 and 14 summarize the optimum number of singular values and their associated stability data. It appears from these results that the solution, when stable, is very unlikely to provide any reasonable approximation of the data. This is seen in two ways: first in the stability data as the number of unstable cases, and secondly in Table 13 by the number of cases selecting one singular value as the optimum.

The case of one singular value, while it does converge, provides no dependable information. Two common profiles observed when too few singular values are selected are to approximate the surface as a single layer or to provide an approximated profile where the layers become cyclical and the depth of the original interface becomes shifted. Figures 21 and 22 provide examples of each the typical profiles when no error is present.

The first example is more common when one singular value is used, while the second example is more common when two singular values are used.

Summary of Smoothing

While the power approximating yielded unstable results, the exponential approximating function appeared very durable when used with the Tyler algorithm. The broad minimum seen when plotting the mean squared error verses the smoothing parameter, α, indicates the mean squared error is not sensitive to small changes in the smoothing parameter. In addition, the level of optimal smoothing was directly related to the error present in the original data. At higher error levels, more something was required to minimize the mean squared error. The predictive criterion appeared to steadily under smooth at overlayers thinner than ~30Å and oversmooth as the overlayer becomes thicker.

The Singular Value Decomposition algorithm gave similar results. Again, the power approximating function was highly unstable and determined not to be a practical alternative to the exponential approximating function. The error in the original data did not a significant effect on the mean squared error when using the exponential approximating function. The optimal number of singular values was consistently either 2 or 3 when more than five measurements were used. The predictive criterion typically selected the same number of singular values.

Table 3. Optimum Smoothing Parameter for Regularization Algorithm using Exponential Function (Equation 13)

Inverse Slope of Interface	Number of Measurements	Percent Error	Mean Depth of Interface 7.5 Å	15 Å	30 Å	60 Å
0.00	3	0%	1.41E-05	1.41E-05	1.48E-04	1.41E-05
0.00	3	1%	1.48E-04	4.80E-04	1.41E-05	1.41E-05
0.00	3	2%	2.67E-04	1.56E-03	1.41E-05	1.41E-05
0.00	3	5%	5.29E-02	5.04E-03	1.41E-05	4.57E-05
0.00	5	0%	1.41E-05	1.41E-05	1.41E-05	1.48E-04
0.00	5	1%	2.67E-04	4.57E-05	2.80E-03	4.80E-04
0.00	5	2%	8.64E-04	2.80E-03	5.04E-03	8.64E-04
0.00	5	5%	2.94E-02	1.63E-02	1.63E-02	1.56E-03
0.00	10	0%	1.41E-05	1.41E-05	1.41E-05	1.41E-05
0.00	10	1%	4.80E-04	8.23E-05	8.64E-04	8.64E-04
0.00	10	2%	1.56E-03	4.80E-04	5.04E-03	1.56E-03
0.00	10	5%	5.29E-02	2.94E-02	1.63E-02	4.80E-04
-18.75	3	0%	1.41E-05	1.41E-05	1.41E-05	1.41E-05
-18.75	3	1%	1.56E-03	8.64E-04	1.41E-05	1.41E-05
-18.75	3	2%	9.07E-03	2.80E-03	1.56E-03	2.54E-05
-18.75	3	5%	9.53E-02	1.63E-02	2.80E-03	8.23E-05
-18.75	5	0%	2.80E-03	8.64E-04	1.41E-05	1.48E-04
-18.75	5	1%	5.04E-03	2.80E-03	5.04E-03	4.80E-04
-18.75	5	2%	1.63E-02	9.07E-03	9.07E-03	1.56E-03
-18.75	5	5%	9.53E-02	2.94E-02	1.63E-02	2.80E-03
-18.75	10	0%	1.41E-05	4.57E-05	1.41E-05	1.41E-05
-18.75	10	1%	9.07E-03	5.04E-03	1.56E-03	8.64E-04
-18.75	10	2%	2.94E-02	1.63E-02	9.07E-03	1.56E-03
-18.75	10	5%	1.71E-01	9.53E-02	2.94E-02	1.56E-03
-37.50	3	0%	N/A	5.04E-03	2.80E-03	1.41E-05
-37.50	3	1%	N/A	9.07E-03	5.04E-03	1.41E-05
-37.50	3	2%	N/A	9.07E-03	5.04E-03	1.41E-05
-37.50	3	5%	N/A	1.63E-02	5.04E-03	1.41E-05
-37.50	5	0%	N/A	1.56E-03	1.41E-05	2.54E-05
-37.50	5	1%	N/A	5.04E-03	5.04E-03	1.56E-03
-37.50	5	2%	N/A	2.94E-02	1.63E-02	2.80E-03
-37.50	5	5%	N/A	5.29E-02	5.29E-02	5.04E-03
-37.50	10	0%	N/A	4.80E-04	8.23E-05	1.41E-05
-37.50	10	1%	N/A	9.07E-03	5.04E-03	1.56E-03
-37.50	10	2%	N/A	2.94E-02	1.63E-02	2.80E-03
-37.50	10	5%	N/A	9.53E-02	5.29E-02	9.07E-03

Table 4. Percent Converged for Regularization Algorithm using Exponential Function (Equation 13)

Inverse Slope of Interface	Number of Measurements	Percent Error	Mean Depth of Interface 7.5 Å	15 Å	30 Å	60 Å
0.00	3	0%	100.00%	100.00%	100.00%	100.00%
0.00	3	1%	99.60%	98.70%	99.80%	100.00%
0.00	3	2%	99.60%	99.60%	94.80%	99.80%
0.00	3	5%	100.00%	99.50%	82.60%	92.50%
0.00	5	0%	100.00%	100.00%	100.00%	100.00%
0.00	5	1%	84.50%	81.80%	99.90%	98.30%
0.00	5	2%	92.00%	98.20%	99.90%	94.20%
0.00	5	5%	99.60%	99.60%	99.60%	77.10%
0.00	10	0%	100.00%	100.00%	100.00%	100.00%
0.00	10	1%	84.70%	69.90%	97.70%	99.60%
0.00	10	2%	93.70%	87.10%	99.90%	98.30%
0.00	10	5%	99.80%	99.90%	99.60%	50.00%
-18.75	3	0%	100.00%	100.00%	100.00%	100.00%
-18.75	3	1%	100.00%	99.90%	99.90%	100.00%
-18.75	3	2%	100.00%	100.00%	98.00%	99.80%
-18.75	3	5%	100.00%	100.00%	88.90%	92.50%
-18.75	5	0%	100.00%	100.00%	100.00%	100.00%
-18.75	5	1%	99.30%	98.30%	100.00%	99.10%
-18.75	5	2%	99.70%	99.60%	99.90%	99.10%
-18.75	5	5%	99.90%	99.90%	99.80%	89.50%
-18.75	10	0%	100.00%	100.00%	100.00%	100.00%
-18.75	10	1%	99.30%	98.90%	98.50%	99.50%
-18.75	10	2%	100.00%	99.80%	99.70%	98.20%
-18.75	10	5%	100.00%	100.00%	100.00%	78.40%
-37.5	3	0%	N/A	100.00%	100.00%	100.00%
-37.5	3	1%	N/A	100.00%	100.00%	100.00%
-37.5	3	2%	N/A	100.00%	99.90%	99.80%
-37.5	3	5%	N/A	100.00%	96.10%	93.00%
-37.5	5	0%	N/A	100.00%	100.00%	100.00%
-37.5	5	1%	N/A	99.60%	100.00%	100.00%
-37.5	5	2%	N/A	99.90%	100.00%	100.00%
-37.5	5	5%	N/A	100.00%	100.00%	97.70%
-37.5	10	0%	N/A	100.00%	100.00%	100.00%
-37.5	10	1%	N/A	99.80%	99.80%	99.90%
-37.5	10	2%	N/A	100.00%	100.00%	99.70%
-37.5	10	5%	N/A	100.00%	100.00%	99.10%

Table 5. Optimum Smoothing Parameter as Predicted by Equation 31 for Regularization Algorithm using Exponential Function (Equation 13)

Inverse Slope of Interface	Number of Measurements	Percent Error	Mean Depth of Interface 7.5 Å	15 Å	30 Å	60 Å
0.00	3	0%	1.41E-05	1.41E-05	2.94E-02	8.64E-04
0.00	3	1%	4.57E-05	4.80E-04	1.63E-02	4.80E-04
0.00	3	2%	8.23E-05	8.64E-04	1.63E-02	1.71E-01
0.00	3	5%	2.67E-04	5.04E-03	5.29E-02	3.09E-01
0.00	5	0%	1.41E-05	8.64E-04	1.41E-05	4.80E-04
0.00	5	1%	2.54E-05	4.80E-04	5.29E-02	2.80E-03
0.00	5	2%	2.67E-04	1.56E-03	5.29E-02	9.07E-03
0.00	5	5%	1.56E-03	5.04E-03	5.29E-02	3.09E-01
0.00	10	0%	2.54E-05	1.41E-05	1.41E-05	8.64E-04
0.00	10	1%	4.57E-05	8.64E-04	2.80E-03	2.80E-03
0.00	10	2%	2.67E-04	2.80E-03	2.94E-02	9.07E-03
0.00	10	5%	8.64E-04	1.63E-02	5.29E-02	5.29E-02
-18.75	3	0%	1.00E+00	1.41E-05	1.41E-05	8.64E-04
-18.75	3	1%	2.54E-05	2.67E-04	2.94E-02	4.80E-04
-18.75	3	2%	1.48E-04	8.64E-04	1.63E-02	1.71E-01
-18.75	3	5%	4.80E-04	2.80E-03	5.29E-02	3.09E-01
-18.75	5	0%	1.00E+00	4.57E-05	1.41E-05	4.80E-04
-18.75	5	1%	2.54E-05	4.57E-05	5.29E-02	2.80E-03
-18.75	5	2%	8.23E-05	1.56E-03	5.29E-02	9.07E-03
-18.75	5	5%	1.56E-03	5.04E-03	5.29E-02	3.09E-01
-18.75	10	0%	4.57E-05	2.54E-05	1.41E-05	8.64E-04
-18.75	10	1%	2.54E-05	1.48E-04	2.80E-03	2.80E-03
-18.75	10	2%	2.67E-04	2.80E-03	2.94E-02	9.07E-03
-18.75	10	5%	8.64E-04	9.07E-03	5.29E-02	5.29E-02
-37.50	3	0%	N/A	1.41E-05	1.56E-03	8.64E-04
-37.50	3	1%	N/A	1.48E-04	2.80E-03	4.80E-04
-37.50	3	2%	N/A	8.64E-04	1.63E-02	1.71E-01
-37.50	3	5%	N/A	2.80E-03	5.29E-02	3.09E-01
-37.50	5	0%	N/A	9.07E-03	1.56E-03	8.64E-04
-37.50	5	1%	N/A	2.54E-05	2.80E-03	2.80E-03
-37.50	5	2%	N/A	8.64E-04	2.80E-03	9.07E-03
-37.50	5	5%	N/A	5.04E-03	5.29E-02	9.53E-02
-37.50	10	0%	N/A	4.57E-05	1.48E-04	8.64E-04
-37.50	10	1%	N/A	1.48E-04	9.07E-03	2.80E-03
-37.50	10	2%	N/A	2.67E-04	1.63E-02	9.07E-03
-37.50	10	5%	N/A	5.04E-03	5.29E-02	5.29E-02

Table 6. Optimum Smoothing Parameter as Predicted by Equation 31 for Regularization Algorithm using Exponential Function (Equation 13)

Inverse Slope of Interface	Number of Measurements	Percent Error	Mean Depth of Interface			
			7.5 Å	15 Å	30 Å	60 Å
0.00	3	0%	100.00%	100.00%	100.00%	100.00%
0.00	3	1%	93.60%	98.70%	100.00%	100.00%
0.00	3	2%	94.70%	97.80%	100.00%	100.00%
0.00	3	5%	95.50%	99.50%	100.00%	100.00%
0.00	5	0%	100.00%	100.00%	100.00%	100.00%
0.00	5	1%	44.90%	94.40%	100.00%	100.00%
0.00	5	2%	79.00%	96.40%	100.00%	100.00%
0.00	5	5%	86.10%	95.60%	99.90%	100.00%
0.00	10	0%	100.00%	100.00%	100.00%	100.00%
0.00	10	1%	52.20%	95.50%	99.20%	99.90%
0.00	10	2%	69.50%	97.40%	100.00%	100.00%
0.00	10	5%	71.00%	99.10%	100.00%	100.00%
-18.75	3	0%	100.00%	100.00%	100.00%	100.00%
-18.75	3	1%	99.50%	99.50%	100.00%	100.00%
-18.75	3	2%	99.00%	99.30%	100.00%	100.00%
-18.75	3	5%	97.60%	98.90%	100.00%	100.00%
-18.75	5	0%	100.00%	100.00%	100.00%	100.00%
-18.75	5	1%	57.80%	89.10%	100.00%	100.00%
-18.75	5	2%	63.10%	98.00%	100.00%	100.00%
-18.75	5	5%	87.40%	97.00%	100.00%	100.00%
-18.75	10	0%	100.00%	100.00%	100.00%	100.00%
-18.75	10	1%	50.30%	80.80%	99.30%	99.90%
-18.75	10	2%	77.50%	98.70%	100.00%	100.00%
-18.75	10	5%	77.20%	98.00%	100.00%	100.00%
-37.5	3	0%	N/A	100.00%	100.00%	100.00%
-37.5	3	1%	N/A	100.00%	100.00%	100.00%
-37.5	3	2%	N/A	99.50%	100.00%	100.00%
-37.5	3	5%	N/A	99.20%	100.00%	100.00%
-37.5	5	0%	N/A	100.00%	100.00%	100.00%
-37.5	5	1%	N/A	87.20%	100.00%	100.00%
-37.5	5	2%	N/A	99.00%	100.00%	100.00%
-37.5	5	5%	N/A	98.10%	100.00%	100.00%
-37.5	10	0%	N/A	100.00%	100.00%	100.00%
-37.5	10	1%	N/A	84.80%	99.90%	100.00%
-37.5	10	2%	N/A	85.50%	100.00%	100.00%
-37.5	10	5%	N/A	97.40%	100.00%	100.00%

Table 7. Optimum Smoothing Parameter for Regularization Algorithm using Power Function (Equation 14)

Inverse Slope of Interface	Number of Measurements	Percent Error	Mean Depth of Interface			
			7.5 Å	15 Å	30 Å	60 Å
0.00	3	0%	Unstable	1.71E-01	1.71E-01	3.09E-01
0.00	3	1%	3.09E-01	3.09E-01	9.53E-02	5.56E-01
0.00	3	2%	1.71E-01	5.56E-01	1.41E-05	1.41E-05
0.00	3	5%	3.09E-01	1.00E+00	5.56E-01	2.67E-04
0.00	5	0%	1.41E-05	4.80E-04	8.23E-05	8.64E-04
0.00	5	1%	Unstable	Unstable	Unstable	Unstable
0.00	5	2%	Unstable	Unstable	Unstable	Unstable
0.00	5	5%	Unstable	Unstable	Unstable	Unstable
-18.75	3	0%	Unstable	5.04E-03	5.29E-02	3.09E-01
-18.75	3	1%	9.53E-02	9.53E-02	5.29E-02	3.09E-01
-18.75	3	2%	1.71E-01	1.71E-01	5.29E-02	5.56E-01
-18.75	3	5%	5.56E-01	5.56E-01	5.56E-01	5.56E-01
-18.75	5	0%	1.41E-05	1.41E-05	8.23E-05	8.64E-04
-18.75	5	1%	Unstable	Unstable	Unstable	Unstable
-18.75	5	2%	Unstable	Unstable	Unstable	Unstable
-18.75	5	5%	Unstable	Unstable	Unstable	Unstable
-37.50	3	0%	N/A	2.80E-03	1.41E-05	1.71E-01
-37.50	3	1%	N/A	9.53E-02	1.41E-05	1.71E-01
-37.50	3	2%	N/A	1.71E-01	2.94E-02	1.71E-01
-37.50	3	5%	N/A	5.56E-01	5.56E-01	5.56E-01
-37.50	5	0%	N/A	2.94E-02	2.54E-05	8.64E-04
-37.50	5	1%	N/A	Unstable	Unstable	5.56E-01
-37.50	5	2%	N/A	Unstable	Unstable	Unstable
-37.50	5	5%	N/A	Unstable	Unstable	Unstable

Table 8. Percent Converged for Regularization Algorithm using Power Function (Equation 14)

Inverse Slope of Interface	Number of Measurements	Percent Error	Mean Depth of Interface 7.5 Å	15 Å	30 Å	60 Å
Infinite	3	0%	Unstable	100.00%	100.00%	100.00%
Infinite	3	1%	20.90%	85.10%	97.90%	50.00%
Infinite	3	2%	37.80%	84.80%	86.50%	97.60%
Infinite	3	5%	43.50%	73.90%	85.00%	87.30%
Infinite	5	0%	100.00%	100.00%	100.00%	100.00%
Infinite	5	1%	Unstable	Unstable	Unstable	Unstable
Infinite	5	2%	Unstable	Unstable	Unstable	Unstable
Infinite	5	5%	Unstable	Unstable	Unstable	Unstable
-18.75	3	0%	Unstable	100.00%	100.00%	100.00%
-18.75	3	1%	44.20%	62.70%	96.90%	100.00%
-18.75	3	2%	48.00%	49.20%	90.10%	90.30%
-18.75	3	5%	60.50%	57.70%	87.40%	54.90%
-18.75	5	0%	100.00%	100.00%	100.00%	100.00%
-18.75	5	1%	Unstable	Unstable	Unstable	Unstable
-18.75	5	2%	Unstable	Unstable	Unstable	Unstable
-18.75	5	5%	Unstable	Unstable	Unstable	Unstable
-37.5	3	0%	N/A	100.00%	100.00%	100.00%
-37.5	3	1%	N/A	58.40%	92.70%	100.00%
-37.5	3	2%	N/A	60.10%	90.20%	99.20%
-37.5	3	5%	N/A	71.30%	86.60%	87.20%
-37.5	5	0%	N/A	100.00%	100.00%	100.00%
-37.5	5	1%	N/A	Unstable	Unstable	45.10%
-37.5	5	2%	N/A	Unstable	Unstable	Unstable
-37.5	5	5%	N/A	Unstable	Unstable	Unstable

Table 9. Optimum Number of Singular Values for Singular Value Decomposition using Exponential Function (Equation 13)

Inverse Slope of Interface	Number of Measurements	Percent Error	Mean Depth of Interface 7.5 Å	15 Å	30 Å	60 Å
0.00	3	0%	2	2	2	2
0.00	3	1%	2	2	2	2
0.00	3	2%	2	2	2	2
0.00	3	5%	2	2	2	2
0.00	5	0%	3	4	4	2
0.00	5	1%	2	3	3	2
0.00	5	2%	2	3	3	2
0.00	5	5%	2	2	3	2
0.00	10	0%	4	4	5	5
0.00	10	1%	2	3	3	2
0.00	10	2%	2	3	3	2
0.00	10	5%	2	3	3	2
-18.75	3	0%	2	2	2	2
-18.75	3	1%	2	2	2	2
-18.75	3	2%	2	2	2	2
-18.75	3	5%	2	2	2	2
-18.75	5	0%	4	3	4	2
-18.75	5	1%	3	3	3	2
-18.75	5	2%	3	3	3	2
-18.75	5	5%	2	2	3	2
-18.75	10	0%	5	5	5	5
-18.75	10	1%	3	3	3	2
-18.75	10	2%	3	3	3	2
-18.75	10	5%	2	2	3	2
-37.50	3	0%	N/A	2	2	2
-37.50	3	1%	N/A	2	2	2
-37.50	3	2%	N/A	2	2	2
-37.50	3	5%	N/A	2	2	2
-37.50	5	0%	N/A	4	4	2
-37.50	5	1%	N/A	3	3	2
-37.50	5	2%	N/A	3	3	2
-37.50	5	5%	N/A	3	3	2
-37.50	10	0%	N/A	4	6	5
-37.50	10	1%	N/A	3	3	2
-37.50	10	2%	N/A	3	3	2
-37.50	10	5%	N/A	2	3	2

Table 10. Percent Converged for Singular Value Decomposition using Exponential Function (Equation 13)

Inverse Slope of Interface	Number of Measurements	Percent Error	Mean Depth of Interface 7.5 Å	15 Å	30 Å	60 Å
0.00	3	0%	100.00%	100.00%	100.00%	100.00%
0.00	3	1%	100.00%	100.00%	100.00%	100.00%
0.00	3	2%	100.00%	100.00%	100.00%	100.00%
0.00	3	5%	99.60%	100.00%	100.00%	100.00%
0.00	5	0%	100.00%	100.00%	100.00%	100.00%
0.00	5	1%	100.00%	72.60%	99.20%	100.00%
0.00	5	2%	100.00%	69.80%	91.90%	100.00%
0.00	5	5%	100.00%	100.00%	51.50%	100.00%
0.00	10	0%	100.00%	100.00%	100.00%	100.00%
0.00	10	1%	100.00%	99.90%	99.90%	100.00%
0.00	10	2%	100.00%	97.80%	99.10%	100.00%
0.00	10	5%	100.00%	68.00%	79.40%	100.00%
-18.75	3	0%	100.00%	100.00%	100.00%	100.00%
-18.75	3	1%	100.00%	100.00%	100.00%	100.00%
-18.75	3	2%	100.00%	100.00%	100.00%	100.00%
-18.75	3	5%	100.00%	100.00%	100.00%	100.00%
-18.75	5	0%	100.00%	100.00%	100.00%	100.00%
-18.75	5	1%	84.40%	99.20%	99.70%	100.00%
-18.75	5	2%	55.80%	87.60%	95.30%	100.00%
-18.75	5	5%	100.00%	100.00%	55.50%	100.00%
-18.75	10	0%	100.00%	100.00%	100.00%	100.00%
-18.75	10	1%	95.00%	100.00%	100.00%	100.00%
-18.75	10	2%	81.30%	99.80%	99.20%	100.00%
-18.75	10	5%	100.00%	100.00%	84.00%	100.00%
-37.5	3	0%	N/A	100.00%	100.00%	100.00%
-37.5	3	1%	N/A	100.00%	100.00%	100.00%
-37.5	3	2%	N/A	100.00%	100.00%	100.00%
-37.5	3	5%	N/A	100.00%	100.00%	100.00%
-37.5	5	0%	N/A	100.00%	100.00%	100.00%
-37.5	5	1%	N/A	100.00%	99.80%	100.00%
-37.5	5	2%	N/A	99.10%	97.30%	100.00%
-37.5	5	5%	N/A	63.50%	63.10%	100.00%
-37.5	10	0%	N/A	100.00%	100.00%	100.00%
-37.5	10	1%	N/A	100.00%	100.00%	100.00%
-37.5	10	2%	N/A	100.00%	99.80%	100.00%
-37.5	10	5%	N/A	100.00%	93.70%	100.00%

Table 11. Optimum Smoothing Parameter as Predicted by Equation 31 for SVD Algorithm using Exponential Function (Equation 13)

Inverse Slope of Interface	Number of Measurements	Percent Error	Mean Depth of Interface 7.5 Å	15 Å	30 Å	60 Å
0.00	3	0%	2	2	2	2
0.00	3	1%	2	2	2	2
0.00	3	2%	2	2	2	2
0.00	3	5%	2	2	2	2
0.00	5	0%	3	3	4	2
0.00	5	1%	3	3	3	2
0.00	5	2%	2	3	3	2
0.00	5	5%	2	2	2	2
0.00	10	0%	3	3	4	2
0.00	10	1%	3	3	2	2
0.00	10	2%	3	3	2	2
0.00	10	5%	2	3	2	2
-18.75	3	0%	2	2	2	2
-18.75	3	1%	2	2	2	2
-18.75	3	2%	2	2	2	2
-18.75	3	5%	2	2	2	2
-18.75	5	0%	3	3	4	2
-18.75	5	1%	3	3	3	2
-18.75	5	2%	3	3	3	2
-18.75	5	5%	1	2	2	2
-18.75	10	0%	3	3	4	2
-18.75	10	1%	3	3	2	2
-18.75	10	2%	3	3	2	2
-18.75	10	5%	1	3	2	2
-37.50	3	0%	N/A	2	2	2
-37.50	3	1%	N/A	2	2	2
-37.50	3	2%	N/A	2	2	2
-37.50	3	5%	N/A	2	2	2
-37.50	5	0%	N/A	3	4	2
-37.50	5	1%	N/A	3	3	2
-37.50	5	2%	N/A	3	3	2
-37.50	5	5%	N/A	3	2	2
-37.50	10	0%	N/A	3	4	2
-37.50	10	1%	N/A	3	4	2
-37.50	10	2%	N/A	3	2	2
-37.50	10	5%	N/A	3	2	2

Table 12. Predicted (Equation 31) Percent Converged using the Optimum Number of Singular Values with the Exponential Approximating Function (Equation 13)

Inverse Slope of Interface	Number of Measurements	Percent Error	Mean Depth of Interface 7.5 Å	15 Å	30 Å	60 Å
0.00	3	0%	100.00%	100.00%	100.00%	100.00%
0.00	3	1%	100.00%	100.00%	100.00%	100.00%
0.00	3	2%	100.00%	100.00%	100.00%	100.00%
0.00	3	5%	99.60%	100.00%	100.00%	100.00%
0.00	5	0%	100.00%	100.00%	100.00%	100.00%
0.00	5	1%	50.20%	72.60%	99.20%	100.00%
0.00	5	2%	100.00%	69.80%	91.90%	100.00%
0.00	5	5%	100.00%	100.00%	100.00%	100.00%
0.00	10	0%	100.00%	100.00%	100.00%	100.00%
0.00	10	1%	83.80%	99.90%	100.00%	100.00%
0.00	10	2%	53.80%	97.80%	100.00%	100.00%
0.00	10	5%	100.00%	68.00%	100.00%	100.00%
-18.75	3	0%	100.00%	100.00%	100.00%	100.00%
-18.75	3	1%	100.00%	100.00%	100.00%	100.00%
-18.75	3	2%	100.00%	100.00%	100.00%	100.00%
-18.75	3	5%	100.00%	100.00%	100.00%	100.00%
-18.75	5	0%	100.00%	100.00%	100.00%	100.00%
-18.75	5	1%	84.40%	99.20%	99.70%	100.00%
-18.75	5	2%	55.80%	87.60%	95.30%	100.00%
-18.75	5	5%	100.00%	100.00%	100.00%	100.00%
-18.75	10	0%	100.00%	100.00%	100.00%	100.00%
-18.75	10	1%	95.00%	100.00%	100.00%	100.00%
-18.75	10	2%	81.30%	99.80%	100.00%	100.00%
-18.75	10	5%	100.00%	75.80%	100.00%	100.00%
-37.5	3	0%	N/A	100.00%	100.00%	100.00%
-37.5	3	1%	N/A	100.00%	100.00%	100.00%
-37.5	3	2%	N/A	100.00%	100.00%	100.00%
-37.5	3	5%	N/A	100.00%	100.00%	100.00%
-37.5	5	0%	N/A	100.00%	100.00%	100.00%
-37.5	5	1%	N/A	100.00%	99.80%	100.00%
-37.5	5	2%	N/A	99.10%	97.30%	100.00%
-37.5	5	5%	N/A	63.50%	100.00%	100.00%
-37.5	10	0%	N/A	100.00%	100.00%	100.00%
-37.5	10	1%	N/A	100.00%	61.20%	100.00%
-37.5	10	2%	N/A	100.00%	100.00%	100.00%
-37.5	10	5%	N/A	89.00%	100.00%	100.00%

Table 13. Optimum Number of Singular Values for Singular Value Decomposition using Power Function (Equation 13)

Inverse Slope of Interface	Number of Measurements	Percent Error	Mean Depth of Interface 7.5 Å	15 Å	30 Å	60 Å
0.00	3	0%	1	2	2	2
0.00	3	1%	2	2	2	2
0.00	3	2%	2	2	2	2
0.00	3	5%	2	2	2	2
0.00	5	0%	1	1	1	2
0.00	5	1%	1	1	1	2
0.00	5	2%	1	1	1	2
0.00	5	5%	1	1	1	2
-18.75	3	0%	1	2	2	2
-18.75	3	1%	2	2	2	2
-18.75	3	2%	2	2	2	2
-18.75	3	5%	2	2	2	2
-18.75	5	0%	1	1	1	2
-18.75	5	1%	1	1	1	2
-18.75	5	2%	1	1	1	2
-18.75	5	5%	1	1	1	2
-37.50	3	0%	N/A	2	2	2
-37.50	3	1%	N/A	2	2	2
-37.50	3	2%	N/A	2	2	2
-37.50	3	5%	N/A	2	2	2
-37.50	5	0%	N/A	1	1	2
-37.50	5	1%	N/A	1	1	2
-37.50	5	2%	N/A	1	1	2
-37.50	5	5%	N/A	1	1	2

Table 14. Percent Converged for Singular Value Decomposition using Power Function (Equation 13)

Inverse Slope of Interface	Number of Measurements	Percent Error	Mean Depth of Interface 7.5 Å	15 Å	30 Å	60 Å
Infinite	3	0%	100.00%	100.00%	100.00%	100.00%
Infinite	3	1%	13.80%	100.00%	100.00%	100.00%
Infinite	3	2%	41.50%	100.00%	100.00%	100.00%
Infinite	3	5%	61.00%	97.20%	100.00%	99.90%
Infinite	5	0%	100.00%	100.00%	100.00%	100.00%
Infinite	5	1%	100.00%	100.00%	100.00%	100.00%
Infinite	5	2%	100.00%	100.00%	100.00%	100.00%
Infinite	5	5%	100.00%	100.00%	100.00%	100.00%
-18.75	3	0%	100.00%	100.00%	100.00%	100.00%
-18.75	3	1%	2.20%	100.00%	100.00%	100.00%
-18.75	3	2%	21.80%	100.00%	100.00%	100.00%
-18.75	3	5%	52.50%	95.30%	100.00%	99.90%
-18.75	5	0%	100.00%	100.00%	100.00%	100.00%
-18.75	5	1%	100.00%	100.00%	100.00%	100.00%
-18.75	5	2%	100.00%	100.00%	100.00%	100.00%
-18.75	5	5%	100.00%	100.00%	100.00%	100.00%
-37.5	3	0%	N/A	100.00%	100.00%	100.00%
-37.5	3	1%	N/A	100.00%	100.00%	100.00%
-37.5	3	2%	N/A	97.20%	100.00%	100.00%
-37.5	3	5%	N/A	87.10%	100.00%	99.90%
-37.5	5	0%	N/A	100.00%	100.00%	100.00%
-37.5	5	1%	N/A	100.00%	100.00%	100.00%
-37.5	5	2%	N/A	100.00%	100.00%	100.00%
-37.5	5	5%	N/A	100.00%	100.00%	100.00%